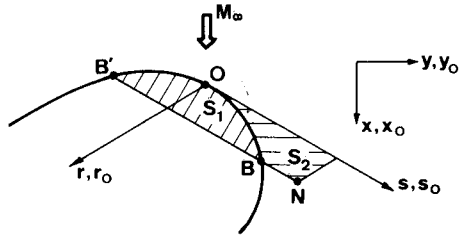

Fig. 1 Regions of integration inside (S_1) and outside (S_2) the wing planform employed in the calculation of the perturbation potential at point N, placed in the wing plane.

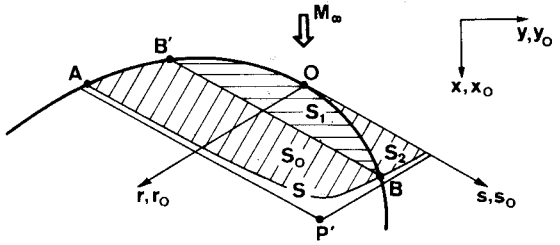

Fig. 2 Regions of integration inside (S_0 and S_1) and outside (S_2) the wing planform employed in the calculation of the perturbation potential at point P, whose projection over the wing plane is P'.

We will show that contributions from S_1 and S_2 cancel each other. To this aim, these contributions can be written as

$$I=-\frac{1}{2\pi\beta}\int_0^{r_B}\frac{\mathrm{d}r_0}{\sqrt{r-r_0}}\left[\int_{s_0=B'O(r_0)}^{s_0=OB(r_0)}\frac{w_i(r_0,s_0)\mathrm{d}s_0}{R}+\int_{s_0=OB(r_0)}^{s_0=S(r_0)}\frac{w_o(r_0,s_0)\mathrm{d}s_0}{R}\right] \tag{6}$$

where $R^2=s-s_0-\tilde{z}^2/(r-r_0)$ and $S(r_0)=s-\tilde{z}^2/(r-r_0)$, as $S(r_0)$ is the value of s_0 for which R vanishes. Equation (6) reduces to

$$I=-\frac{1}{2\pi\beta}\int_0^{r_B}\frac{\mathrm{d}r_0}{\sqrt{r-r_0}}\left[\int_{s_0=B'O(r_0)}^{s_0=OB(r_0)}\frac{w_i(r_0,s_0)\mathrm{d}s_0}{\sqrt{S(r_0)-s_0}}+\int_{s_0=OB(r_0)}^{s_0=S(r_0)}\frac{w_o(r_0,s_0)\mathrm{d}s_0}{\sqrt{S(r_0)-s_0}}\right] \tag{7}$$

The integral I is zero because the terms within the brackets coincide with Eq. (4). This term states that ψ is zero at the point $[r_0,S(r_0)]$, which is placed over the part of the hyperbola S lying outside the planform. Therefore, S_0 is the only region contributing to the integral in Eq. (5). The effect of the source points placed in the regions S_1 and S_2 is to cancel each other. This occurs because along each line $r_0=$ constant of the region of integration, the relationship (4) guarantees the compensation of effects produced on P by both segments of this line lying in S_1 and S_2, respectively.

Once the cancellation zone is determined, the velocity perturbation component u can be calculated in the usual way[1-4] and the extension to the calculation of u at a point influenced by the wing wake produced at a subsonic trailing edge is obvious.

References

[1]Evvard, J. C., "Use of Source Distributions for Evaluating Theoretical Aerodynamics of Thin Finite Wings at Supersonic Speed," NACA Rept. 951, 1950.

[2]Krasilshchikova, E. A., "Finite Span Wings in Compressible Flow," NACA TM 1383, 1956.

[3]Krasilshchikova, E. A., *A Thin Wing in a Compressible Flow*, Mir Publishers, Moscow, 1982, pp. 31-37.

[4]Jones, R. T. and Cohen, D., "Aerodynamics of Wings at High Speeds," *High Speed Aerodynamics and Jet Propulsion*, Vol. VII, Princeton, NJ, 1957, pp. 174-183.

Transonic Airfoil Calculations Including Wind Tunnel Wall-Interference Effects

L. S. King* and D. A. Johnson*
NASA Ames Research Center
Moffett Field, California

Introduction

MEANINGFUL comparisons of experiment and Navier-Stokes calculations for airfoils at transonic speeds require a proper account of wind tunnel wall interference effects. Levy[1] demonstrated this by using a tangency condition at the walls of a solid-wall tunnel. King and Johnson[2] employed a pressure boundary condition utilizing measured pressures in the flowfield as boundary data. In both cases, inclusion of wall-interference effects resulted in shock positions close to that observed experimentally. Free-air results characteristically placed the shock too far downstream.

While qualitatively correct, the results of Ref. 2 were unsatisfactory because of the finite-difference meshes employed. In particular, surface pressures exhibited significant irregularities that were mesh dependent and which limited interpretation of the results. The purpose of this Note is to present additional calculations performed on finer, better designed meshes, so that a truer representation of wall effects may be demonstrated.

Numerical Procedure

The basic technique employed is the numerical method developed by Steger[3] for the Reynolds-averaged time-dependent compressible Navier-Stokes equations. The method comprises the following elements: 1) transformation of the governing equations to a generalized body-fitted coordinate system; 2) the thin-layer approximation for the viscous terms; 3) the algebraic turbulence model of Baldwin and Lomax[4]; and 4) use of the second-order-accurate factored-implicit algorithm of Beam and Warming.[5,6]

To account for wind tunnel wall interference, the Steger code was modified by incorporating a pressure boundary condition (PBC) along the upper and lower computational boundaries. The pressures imposed are those measured experimentally at locations one chord above and below the airfoil. Because the flows for the conditions tested were entirely subsonic at these locations, inviscid homentropic flow is a reasonable assumption. Using the notation of Steger,[3] the equations along the outer boundary are

$$p/p_\infty=(p/p_\infty)_{\text{meas}} \tag{1}$$

$$\rho=(p/p_\infty)^{1/\gamma} \tag{2}$$

$$\tfrac{1}{2}(u^2+v^2)=(1-a^2)/(\gamma-1)+\tfrac{1}{2}u_\infty^2 \tag{3}$$

Received May 5, 1984; revision received March 25, 1985. This paper is declared a work of the U. S. Government and is not subject to copyright protection in the United States.

*Research Scientist. Member AIAA.

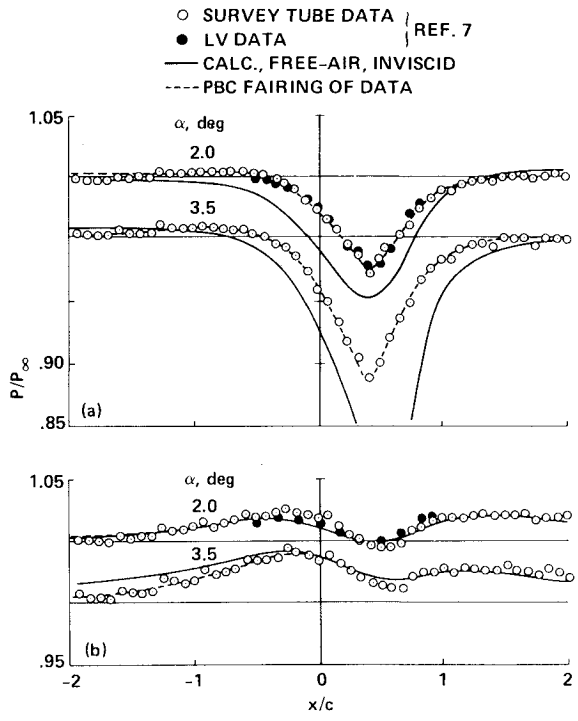

Fig. 1 Flowfield pressure distributions: a) one chord above airfoil; b) one chord below airfoil.

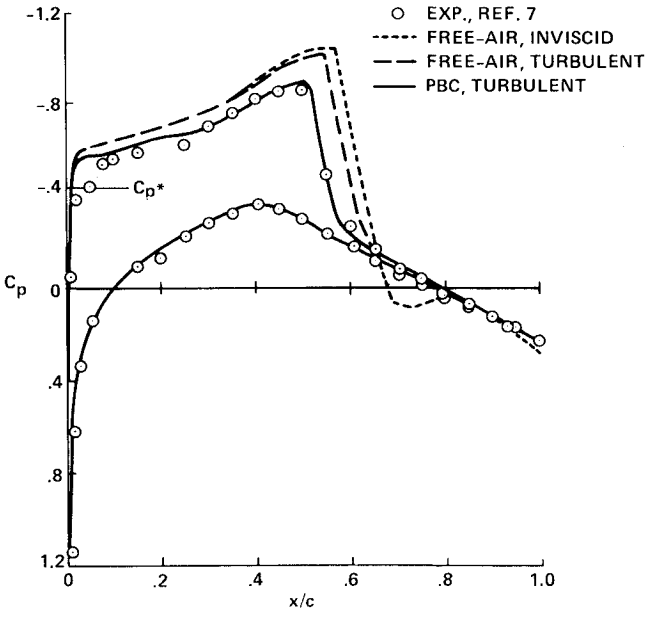

Fig. 2 Airfoil surface pressures for $M_\infty = 0.8$ and $\alpha = 2$ deg.

$$\partial_t J^{-1}\rho v = -\partial_\xi J^{-1}(\rho vU + \xi_y p) - \partial_\eta J^{-1}(\rho vV + \eta_y p) \qquad (4)$$

Because flow is permitted across the boundary, the momentum equation (4) is solved for the vertical velocity (v) by using central differences for the ξ derivative and one-sided interior differences for the η derivative. Conditions along the boundary are determined after the interior points have been updated, so that a simple tridiagonal system results for the boundary difference equations.

Results and Discussion

The calculations were performed at the test conditions reported in Ref. 7. These data were obtained in the Ames

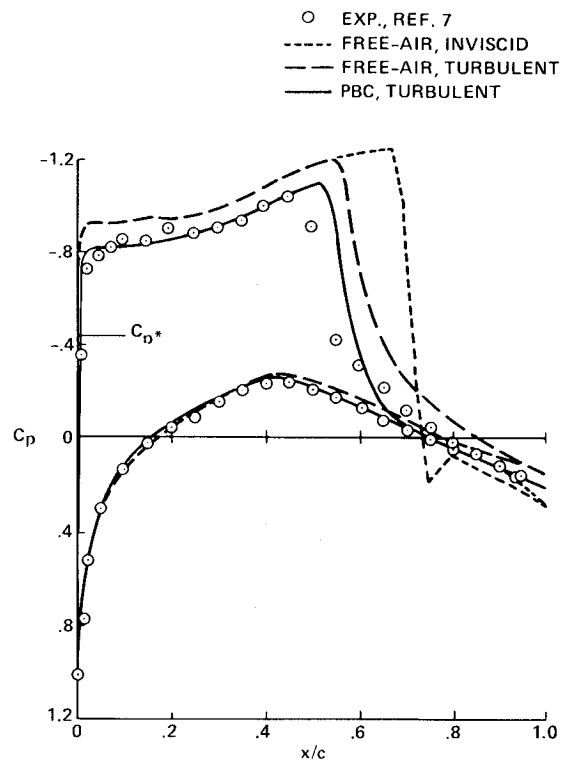

Fig. 3 Airfoil surface pressures for $M_\infty = 0.8$ and $\alpha = 3.5$ deg.

2×2 Foot Transonic Wind Tunnel on a 6 in. (15.24 cm) chord NACA 64A010 airfoil. The Reynolds number for the test was 2×10^6 based on chord and freestream velocity. Test conditions selected for comparison of the calculations with experimental data were: 1) Mach number M_∞ of 0.8 at a geometric angle of attack, α, of 2 deg, and 2) $M_\infty = 0.8$ and $\alpha = 3.5$ deg. The flow is attached for the first set of test conditions; a small separation bubble exists for the second set.

In Ref. 2 the turbulent PBC calculations were obtained on 97×35 meshes. Subsequent calculations have been performed on 137×50 meshes, in which care was exercised in resolving the nose, shock, and trailing-edge regions. The mesh generation code used the clustering method of Steger and Sorenson[8] in an elliptic solver. In the calculations, steady state was assumed to have been achieved when the lift coefficient changed by less than .0001 over the time required for a freestream particle to travel one chord. Using the nonvectorized version of the code, typical run times on the Cray 1S were about 45 min for a turbulent case and about 12 min for an inviscid case.

Shown in Fig. 1 are the measured flowfield pressure distributions along $y/c = \pm 1.0$ for the two sets of conditions for which computations have been made and the corresponding predictions for an unbounded inviscid flow. Figure 1a shows the results above the airfoil, and Fig. 1b shows those below the airfoil. The data in Fig. 1 are displayed on a greatly expanded scale because the flowfield pressures everywhere are near the freestream value. The small differences are significant, however, because of the sensitivity of transonic flows. For example, at $M_\infty = 0.8$ and $\alpha = 2$ deg, the measured pressures and the calculated free-air inviscid pressures at the measurement position have a maximum difference of about 1% of free stream, yet yield significantly different results on the airfoil surface, as seen in Fig. 2.

Figures 2 and 3 compare calculated surface pressures with experimental results. For each test condition three calculations are shown: two free-air solutions (inviscid and tur-

bulent) and a turbulent PBC calculation. These allow an assessment of the relative importance of viscous effects and wall effects for the two flows. For the attached flow (Fig. 2), viscous effects exert little influence on shock position and trailing-edge pressure recovery, the main viscous effect being a smoothing of the overcompression at the foot of the shock. Also, there is a slight (2% chord) forward positioning of the shock due to the viscous effects. Once the flow separates, however, viscous effects on the surface pressures are significant, as seen in Fig. 3. A comparison of the two free-air calculations shows the shock position for the turbulent solution to be about 9% chord upstream of the inviscid position. Trailing-edge pressure recovery is also significantly reduced in the turbulent solution.

On the upper surface of the airfoil none of the free-air solutions are close to the experimental data at either test condition. Imposition of the measured pressures on the upper and lower computational boundaries dramatically improves this situation. For the attached flow (Fig. 2), the turbulent PBC solution shows excellent agreement with the data, the main effect of the PBC being a forward positioning of the shock to the experimental location. For a flow with a separation bubble (see Fig. 3), the PBC moves the shock forward, but still downstream of the measured position. It appears that deficiencies in the turbulence model for describing separated flows are responsible for the lack of agreement, although mesh resolution may still be a factor.

Conclusion

For attached flows, the pressure boundary condition has been demonstrated to be effective in accounting for wind tunnel wall-interference effects in numerical calculations. Surface-pressure results also agree well with experiment for this situation. For separated flows, however, turbulent PBC calculations show an improvement over free-air solutions even though inadequacies in the turbulence modeling are still important limitations. Evaluation of turbulence models for separated airfoil flows could benefit from using the Reynolds-averaged Navier-Stokes code with the pressure boundary condition and appropriate experimental data.

References

[1]Levy, L. L., Jr., "Experimental and Computational Steady and Unsteady Transonic Flows about a Thick Airfoil," *AIAA Journal*, Vol. 16, June 1978, pp. 564-572.

[2]King, L. S. and Johnson, D. A., "Calculations of Transonic Flow about an Airfoil in a Wind Tunnel," AIAA Paper 80-1366, 1980.

[3]Steger, J. L., "Implicit Finite-Difference Simulation of Flow about Arbitrary Two-Dimensional Geometries," *AIAA Journal*, Vol. 16, July 1978, pp. 679-686.

[4]Baldwin, B. S. and Lomax, H., "Thin Layer Approximation and Algebraic Turbulence Model for Separated Turbulent Flows," AIAA Paper 78-257, 1978.

[5]Beam, R. and Warming, R. F., "An Implicit Finite-Difference Algorithm for Hyperbolic Systems in Conservation-Law Form," *Journal of Computational Physics*, Vol. 22, Sept. 1976, pp. 87-110.

[6]Beam, R. and Warming, R. F., "An Implicit Factored Scheme for the Compressible Navier-Stokes Equations," *AIAA Journal*, Vol. 16, April 1978, pp. 393-402.

[7]Johnson, D. A. and Bachalo, W. D., "Transonic Flow Past a Symmetrical Airfoil-Inviscid and Turbulent Flow Properties," *AIAA Journal*, Vol. 18, Jan. 1980, pp. 16-24.

[8]Steger, J. L. and Sorenson, R. L., "Automatic Mesh-Point Clustering Near a Boundary in Grid Generation with Elliptic Partial Differential Equations," *Journal of Computational Physics*, Vol. 33, Dec. 1979, pp. 405-410.

Effect of Blunt Trailing Edge on Rotor Broadband Noise

S.-T. Chou* and A. R. George†
Cornell University, Ithaca, New York

TURBULENT vortex shedding from blunt trailing edges is a source of rotor high-frequency broadband noise.[1] Brooks and Hodgson[2] were the first to demonstrate the importance of this self-noise mechanism for stationary airfoils. In their experiment with an isolated airfoil, they found that the radiated noise increased significantly for airfoils with thickened trailing edges. This Note studies the parametric dependence of this noise mechanism and develops a method to predict rotor broadband noise associated with turbulent vortex shedding from blunt trailing edges.

Blunt trailing-edge noise radiation is a result of higher surface presssure fluctuations near the airfoil's trailing edge due to turbulent vortex shedding. To predict this noise mechanism, our first task is to scale the fluctuating surface pressures. Using dimensional analysis or physical reasoning, the following relationships for the parametric dependence for S_{pp} and f were found

$$S_{pp} \sim q^2 t^3 / U, \qquad f \sim U/t$$

where S_{pp} is the power spectral density of surface pressure fluctuation, f the frequency, q the dymanic pressure ($\rho U^2/2$), t the trailing-edge thickness, and U the freestream velocity. By using the above relationships, the surface pressure spectrum S_{pp} is assumed to have the following form

$$S_{pp}(f) = q^2 t^3 S_0(\tilde{\omega})/U$$

where $\tilde{\omega} = 2\pi f t/U$. The normalized spectrum $S_0(\tilde{\omega})$ can be found empirically from experimental data. Due to the lack of measurements for surface pressure fluctuation near blunt trailing edges, such data were obtained by inverting the acoustic data measured by Brooks and Hodgson[2] using their stationary airfoil analysis. Using the above scaling relation, the data representing a wide range of freestream velocities and trailing-edge thickness are collapsed reasonably well to a single curve. By using curve-fitting techniques, the empirical expression for the normalized spectrum S_0 is found in terms of $\sigma = \log_{10}\tilde{\omega}$ as follows:

$$\log_{10} S_0(\tilde{\omega}) = 17.394 - 106.57\sigma - 158.12\sigma^2 + 99.27\sigma^3 - 33.249\sigma^4 + 16.721\sigma^5$$

for $0.2 < \sigma < 2$, otherwise

$$S_0(\tilde{\omega}) = 0$$

Figure 1 shows the fitted curve along with the experimental data.

To predict the additional broadband noise radiation from a rotor due to its blunt trailing edge, several assumptions have to be made. First the source is modeled as rotating radiating dipoles, and the rotor/observer relative position is

Received Nov. 8, 1985.

*Graduate Research Assistant, Sibley School of Mechanical and Aerospace Engineering. Student Member AIAA.

†Professor and Director, Sibley School of Mechanical and Aerospace Engineering. Associate Fellow.